Electronic Supplementary Information
to
Theoretical Insight into Origin of Electrochemical Promotion of Ethylene oxidation on Ruthenium Oxide

*Yasmine M. Hajar[1], Laureline Treps[2], Carine Michel[2], Elena A. Baranova,[1] Stephan N. Steinmann[2]**

[1]Department of Chemical and Biological Engineering, Centre for Catalysis Research and Innovation (CCRI), University of Ottawa, 161 Louis-Pasteur, Ottawa, ON K1N 6N5, Canada. E-mail: elena.baranova@uottawa.ca; Tel: 16135625800 (x 6302); Fax: 16135625172.

[2]Univ Lyon, ENS de Lyon, CNRS, Université Lyon 1, Laboratoire de Chimie UM R 5182, F-69342, Lyon, France. E-mail: stephan.steinmann@ens-lyon.fr; Fax: +33472728080; Tel: +33472728847

Table of Contents

1. Reactor design

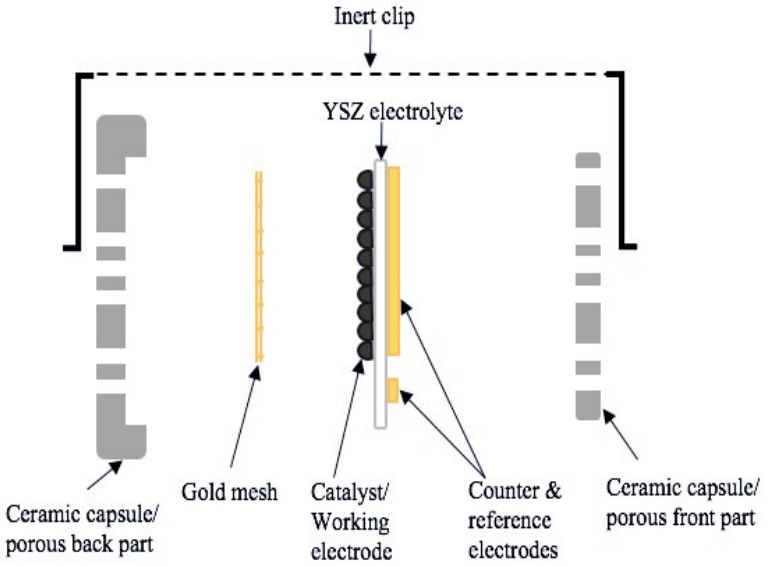

Figure S 1: Schematic of the electrochemical cell showing the electrolyte, the working electrode WE, counter electrode CE and reference electrode RE sandwiched in a ceramic capsule.

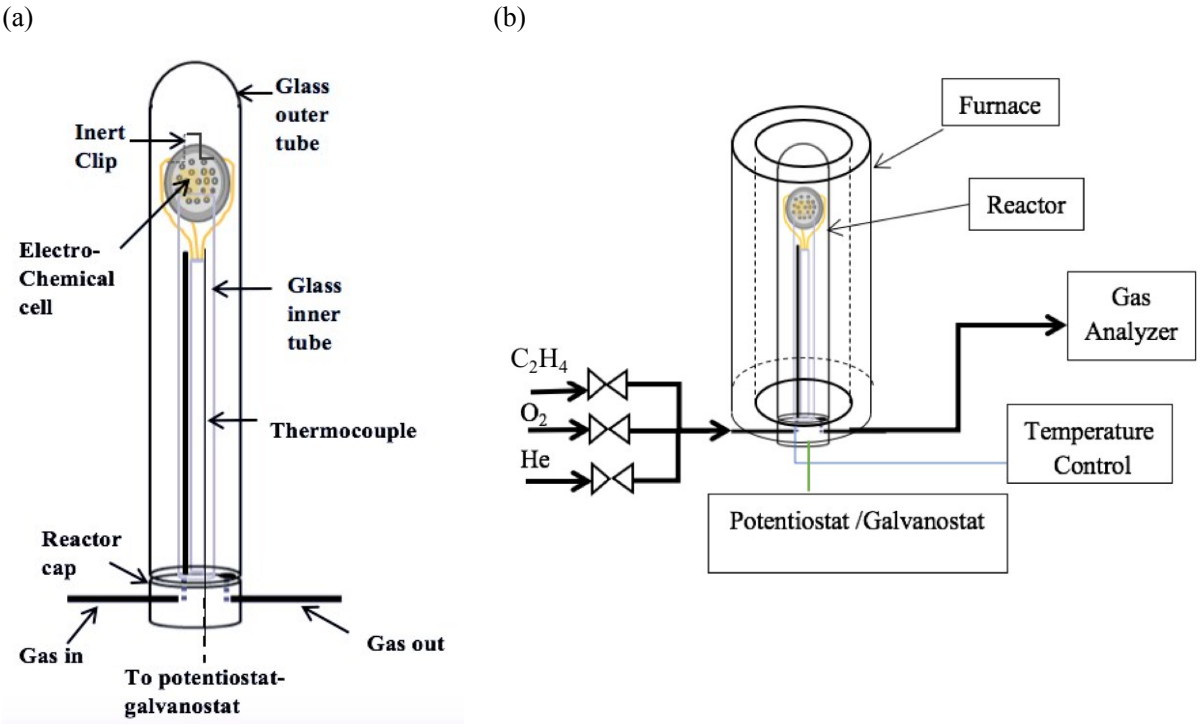

Figure S 2: (a) Schematics of the quartz reactor showing the suspended the electrochemical cell and (b) Schematic of the overall experimental apparatus for EPOC experiments.

2. Typical result from electrochemical promotion of catalysis experiment

Figure S 3 shows a typical electrochemical promotion of catalysis result when applying a constant current. In here for example a current of 100 μA is applied, following Faraday's law the value of r_{elec} would be the expected new value based on the electrochemical reaction occurring; however, an increase in the rate to a new value r occurs, defying the Faraday's law and hence the promotion is called non-Faradaic. As explained in the manuscript, the increase in the rate to higher values is due to change in adsorption strength and decrease of activation energy, upon potential application.

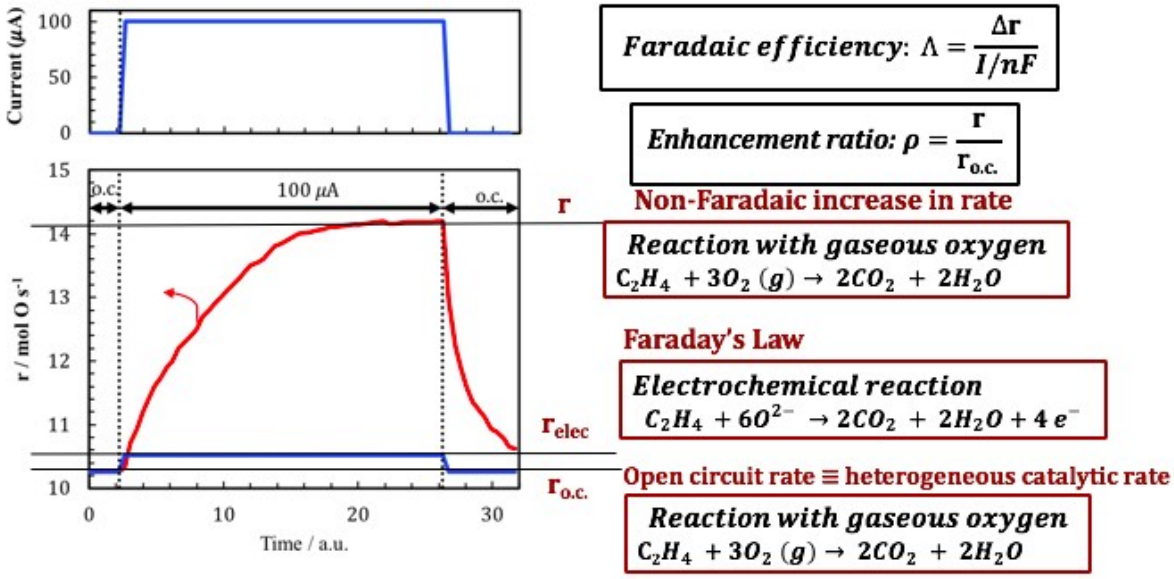

Figure S 3: Typical change in the rate of reaction (r_{oc} to r) upon application of a constant current vs the expected increase due to the electrochemical reaction (r_{elec}).

3. Cyclic voltammetry effect on catalytic rate

An additional cyclic voltammetry test was performed to show the on-line enhancement in the catalytic rate as a function of the potential applied. The current response as well as the catalytic rate are shown in Figure S 4. A potential window range between -0.8 and 0.8 V was set and the scan rate used was 2 mV/s. Upon the increase in potential in the [+0 V – +0.8 V] range, the catalytic rate can be seen gradually increasing concomitantly with the current increase up to 107 μA; this was followed by a short stabilization of the catalytic rate before it started dropping back to its initial catalytic open circuit (o.c.) rate. Upon the start of the cathodic range of the CV, an increase in the catalytic rate resurfaced, proving the inverted-volcanic EPOC effect on RuO_2.

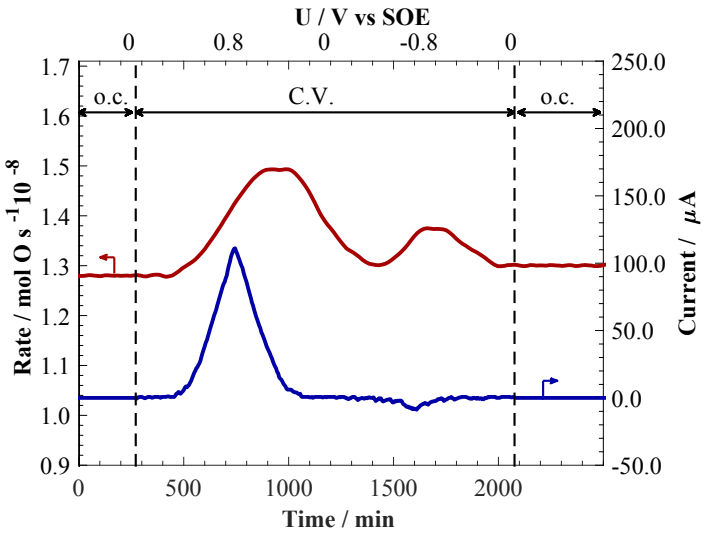

Figure S 4: Transient rate response of RuO_2 NPs to cyclic voltammetry in the [-0.8V – 0.8V]. open-circuit. Conditions: T = 350 °C, $P_{C_2H_4}$ = 0.012 kPa, P_{O_2}=3 kPa. Total flow rate = 100 ccm.

4. Ab Initio atomistic thermodynamics

Thermodynamic stability of a surface can be derived by comparing a multitude of surface structures and their corresponding surface free energy (SFE) $\gamma\left(T,P_{O_2}\right)$. The surface with the lowest SFE is the most stable structure. Two main variables that are required for the calculation of RuO_2 (110) surface free energy are temperature (*T)* and oxygen partial pressure (P_{O_2}). The environment in which RuO_2 surface is tested has constant *T* and P_{O_2} regardless of the exchange that occurs between surface and the environment (acting as a reservoir). The system's Gibbs free energy *G* is essential to such calculations as it represents the thermodynamic potential of the system with a dependency on the number of atoms of Ru and O (N_{Ru} and N_O), P_{O_2} and *T*. The free surface energy calculated to find the most stable surface composition and geometry is defined as follows based on the work of Reuter *et al.* [1] (Equation S 1):

$$\gamma\left(T,P_{O_2},N_{Ru},N_O\right)=\frac{1}{2S}\left\{G^{slab}_{RuO_2\left(T,P_{O_2},N_{Ru},N_O\right)}-N_{Ru}\,\mu_{Ru\left(T,P_{O_2}\right)}-N_O\mu_{O\left(T,P_{O_2}\right)}\right\} \qquad \text{Equation S 1}$$

where the chemical potentials of Ru and O are μ_{Ru} and μ_O, and N_{Ru} and N_O are the number of Ru and O atoms in the three-dimensional supercell. SFE is normalized by dividing by the total surface area 2*S* of the two symmetrical sides in the unit cell plane direction.

The bulk material available in the slab acts as a thermodynamic reservoir and relates the chemical potentials of Ru and O; therefore, allowing the substitution of the chemical potential of Ru by its relation to the Gibbs free energy of bulk oxide, $g^{bulk}_{RuO_2}$. Since in experimental settings it is the partial pressure of O_2

molecule that is controlled, SFE becomes a function of μ_{O_2}. In addition, the influence of temperature and pressure are negligible on solids; therefore, the Gibb's energy of the bulk will be considered equal to the electric energy computed for the primitive cell of the bulk $e^{bulk}_{RuO_2}$. Similarly, the free energy of the surface $G^{slab}_{RuO_2}$is considered equivalent to its electric energy $E^{slab}_{RuO_2}$. This results in SFE being equal to Equation S 2:

$$\gamma\left(T,P_{O_2},N_{Ru},N_O\right)=\frac{1}{2S}\left\{E^{slab}_{RuO_2(N_{Ru},N_O)}-N_{Ru}\,e^{bulk}_{RuO_2}+\left(2\,N_{Ru}-N_O\right)\frac{1}{2}\mu_{O_2\left(T,P_{O_2}\right)}\right\} \quad \text{Equation S 2}$$

The chemical potential of oxygen μ_{O_2} is then described as a function of the standard chemical potential $\mu^o_{O_2}$, T and P_{O_2} as follows (Equation S 3):

$$\mu_{O_2\left(T,P_{O_2}\right)}=\mu^o_{O_2(T,P^o)}+RTln\frac{P_{O_2}}{P^o_{O_2}} \quad \text{Equation S 3}$$

The standard chemical potential of an oxygen molecule within the ideal gas approximation is equal to its Gibbs free energy ($g^{gas}_{O_2(T,P^o)}$). Directly expressing the oxygen Gibbs free energy in terms of an electronic internal energy does not result in accurate values when using GGA functionals [2]. Therefore, the oxygen Gibbs free energy is derived from the water formation reaction. The Gibbs free energy of oxygen is related to the Gibbs free energy of water formation and the Gibbs free energies of hydrogen and water at standard conditions (Equation S 4).

$$\mu^o_{O_2(T,P^o)}\approx g^{gas}_{O_2\left(T,P^o_{O_2}\right)}=-2\,\Delta G^f_{H_2O}+2\,g^{gas}_{H_2O\left(T,P^o_{H_2O}\right)}+2\,g^{gas}_{H_2\left(T,P^o_{H_2}\right)} \quad \text{Equation S 4}$$

4.1 Surface potential effect on the ab initio atomistic thermodynamics

The electrochemical promotion effect on the catalyst slab electric energy was modeled by adding the Poisson-Boltzmann equation [3,4] to the general Kohn-Sham equation using the VASPsol module [5]. The solution to the new equation is added to the electronic ground state resulting in a modification of the total free energy and forces. This method has been validated for the adsorption of pyridine on Au (111) by Steinmann *et al.* [6]. The implicit solvation model places a quantum-mechanical solute in a cavity surrounded by a continuum dielectric description of the solvent [7,8]. The relative permittivity of the solvent used tested in Figure S 13, while the cavity size effect is demonstrated in Figure S 12. Both have been shown to have a negligible effect on the SFE value for the three possible surface termination ($2O^{br}/2O^{ot}$, $2O^{br}/2Ru$ and $2Ru/2Ru$).

In the previous SFE equation, the oxygen supply is gaseous, whereas in EPOC conditions, the oxygen is supplied in its ionic form from the oxygen-conducting electrolyte material as follows (Equation S 5):

$$O^{2-}(YSZ) + RuO_2 \rightarrow O@RuO_2 + 2e^- \quad \text{Equation S 5}$$

The chemical potentials of gaseous oxygen μ_O is replaced by that of oxygen anion $\mu_{O^{2-}}$ and the corresponding SFE equation is described as follows (Equation S 6).

$$\gamma(T,P,N_{Ru},N_O,U_{anode/SHE}) = \frac{1}{2S}\left\{E^{slab}_{RuO_2(N_{Ru},N_O,U)} - N_{Ru}\,e^{bulk}_{RuO_2} + (2N_{Ru} - N_O)\,\mu_{O^{2-}(} \right. \quad \text{Equation S 6}$$

The chemical potential of oxygen anions $\mu_{O^{2-}}$ is linked through Equation S 7 with the chemical potential of oxygen from the gas phase and the potential applied versus a Standard Oxygen Electrode (SOE).

$$\begin{aligned}\mu_{O^{2-}} &= \frac{1}{2}\mu_{O_2} + 2eU_{anode/SOE} \\ &= \frac{1}{2}\mu_{O_2} + 2e(U_{anode/vac} + U_{vac/SOE}) \\ &= \frac{1}{2}\mu_{O_2} + 2e(U_{anode/SHE} + U_{SHE/vac} + U_{vac/SOE}) \\ &= \frac{1}{2}\mu_{O_2} + 2e(U_{anode/SHE} + U_{SHE/SOE})\end{aligned} \quad \text{Equation S 7}$$

It has been established that the equilibrium potential of SOE with respect to vacuum is 5.14 V [9], whereas that of SHE is 4.44 V [10]; therefore the equilibrium potential of SHE with respect to SOE is equal to -0.7 V and the SFE equation as a function of potential vs SHE is as follows (Equation S 8).

$$\begin{aligned}&\gamma\left(T,P_{O_2},N_{Ru},N_O,U_{anode/SHE}\right) \\ &\quad = \frac{1}{2S}\left\{E^{slab}_{RuO_2(N_{Ru},N_O,U_{anode/SHE})} - N_{Ru}\,e^{bulk}_{RuO_2} \right. + \end{aligned} \quad \text{Equation S 8}$$

5. Additional Figures and Sensitivity analysis on numerical setting

5.1 Effect of chemical potential, temperature and oxygen partial pressure

Before investigation of the potential effect on the nature of the surface termination, calculation for the effect of oxygen chemical potential on the surface free energy was performed to show that under open-circuit potential, the surface with $2O^{br}/2O^{ot}$ is the most stable surface termination (Figure S 5). The results we obtained are in agreement with the findings of Reuter *et al.* [1]. Furthermore, Figure S 6 shows the

change of the surface termination at ocp as a function of temperature and oxygen partial pressure. This proves the stability of the $2O^{br}/2O^{ot}$ for the experimental pressure and temperature range.

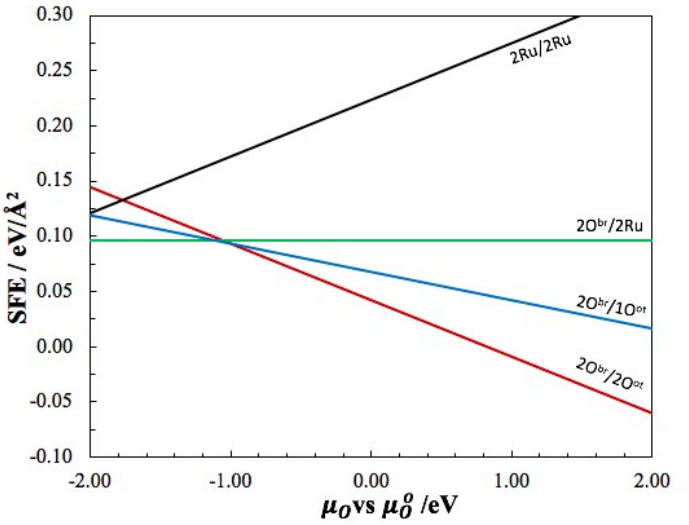

Figure S 5: Surface free energy of RuO_2 (110) as a function of chemical potential at 350 °C vs standard chemical potential, under open-circuit potential conditions.

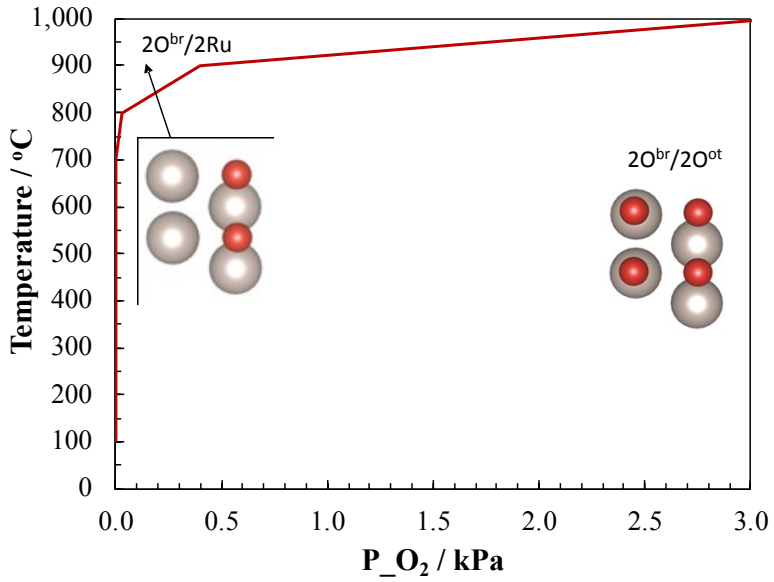

Figure S 6: RuO_2 (110) phase diagram as a function of temperature and oxygen partial pressure, under open-circuit potential conditions.

To clarify better the minimal effect of oxygen partial pressure, Figure S 7a&b compares the SFE values as a function of electric potential applied under 1 kPa of oxygen partial pressure in (a) and under10^{-10} kPa in (b). The point at which the transition occurs from one state to another shifts slightly between the two figures proving the limited effect of partial pressure of O_2 on the phase diagram.

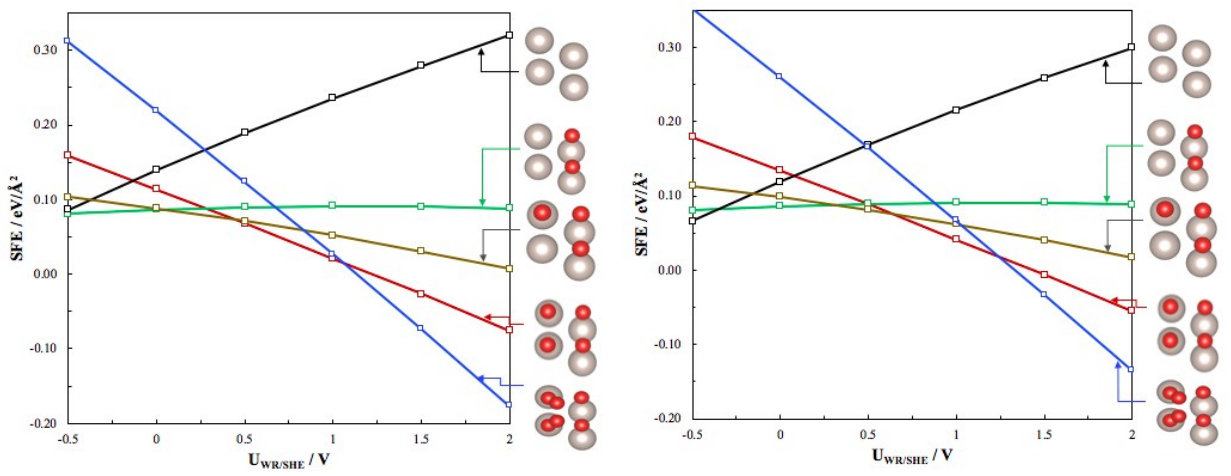

(a) (b)

Figure S 7: Surface free energy of RuO_2 (110) as a function of electrical potential applied at 350 ° C at a partial pressure of oxygen of (a) 1 kPa (experimental and (b) 10^{-10} kPa (ultra-high vacuum chamber conditions).

5.2 Effect of Number of Ru layers

The number of Ru atoms layers was varied between 2 and 6 layers and the surface free energy was calculated for a unit cell (Figure S 8a). It can be seen that the surface energy was stable as a function of the number of Ru layers confirming that the size of the unit cell used does not wrongly effect our calculations. Similarly, adsorption energy of ethylene and oxygen on the most stable surface position was calculated as a function of the number of Ru layers; this confirmed as well the choice of 3 layers of Ru (Figure S 8b).

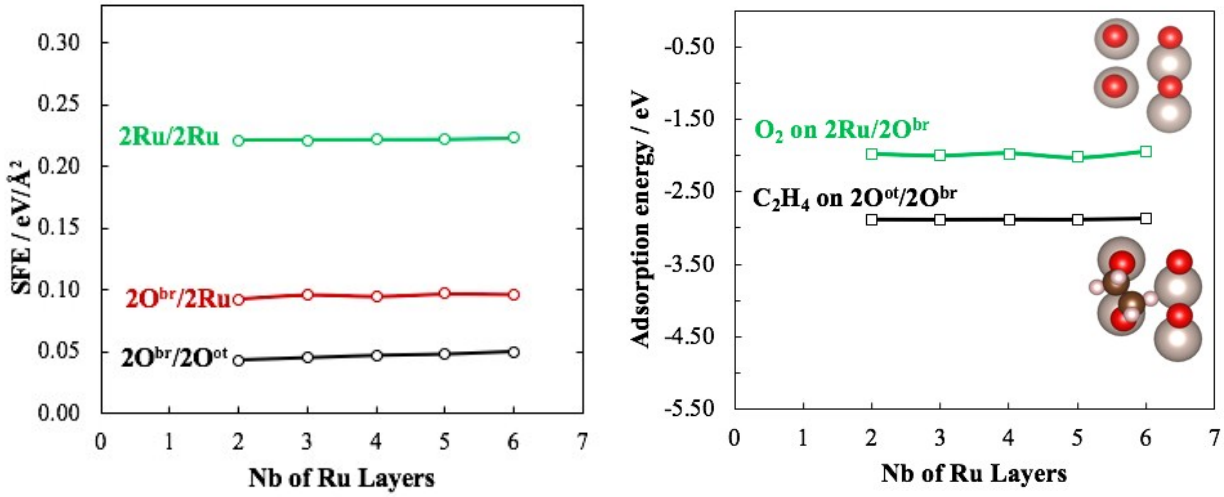

(a) (b)

Figure S 8: Effect of number of Ru layers on (a) the surface energy for $2O^{br}/2O^{ot}$, $2O^{br}/2Ru$ and 2Ru/2Ru surface termination of RuO_2 (110) surface and (b) on the adsorption energy of ethylene and oxygen molecules on the most stable position.

5.3 Vacuum effect test

Vacuum test was performed on the RuO_2 slab with $2O^{br}/2O^{ot}$, $2O^{br}/2Ru$ and 2Ru/2Ru surface termination by varying the vacuum in the range of 15 to 30 Å in z-direction. Figure S 9 demonstrates SFE under 15 and 30 Å only and it can be seen that there is an insignificant change in the SFE value as a function of vacuum length, which confirms the use of 15 Å of vacuum length in our calculations.

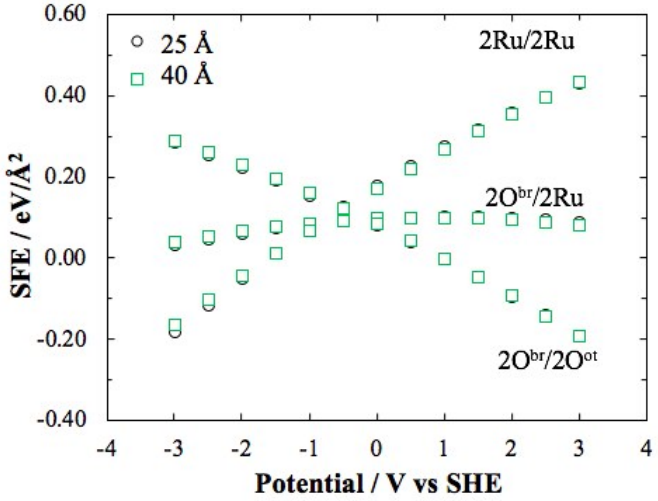

Figure S 9: Vacuum thickness effect on SFE value for $2O^{br}/2O^{ot}$, $2O^{br}/2Ru$ and 2Ru/2Ru surface termination of RuO_2 (110) surface.

5.4 Energy cut-off effect

The effect of energy cut-off on the variation of the slab energy is depicted in

Figure S 10, showing that a value of 550 eV is large enough to converge the Fourier series set used in our DFT calculations.

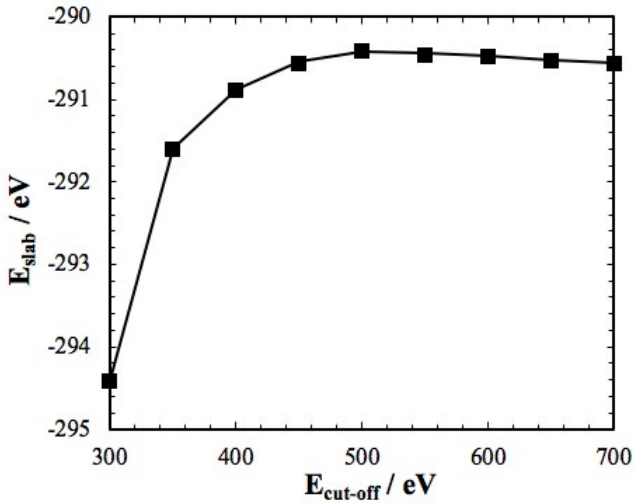

Figure S 10: Slab energy variation as a function of energy cut-off value, at K-points value of 6x6x1 for $2O^{br}/2O^{ot}$ surface termination of RuO_2 (110) surface.

5.5 Charge effect on potential and work function value

Figure S 11 serves as a confirmation to the charge addition/removal effect on the three systems' work function and corresponding potential. It can be seen that the removal of charges corresponds to an anodic behavior such as the potential value increases along with the work function value. In addition, there is an increasing work function value as a function of presence of more O^{ot} atoms when changing systems from 2Ru/2Ru to $2O^{br}$/2Ru to $2O^{br}/2O^{ot}$.

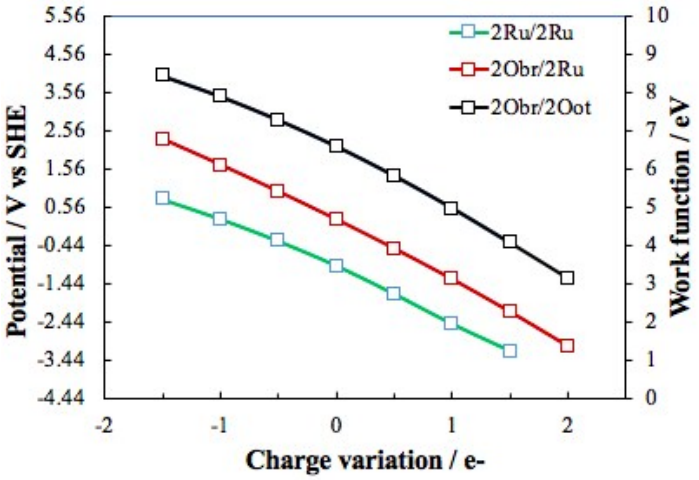

Figure S 11: Charge removal/addition effect on the potential value and work function value.

5.6 Relative permittivity test

Similarly, the relative permittivity test showed minimal variation in SFE as a function of the ε_r used, confirming the use of ε_r =79 corresponding to water solvent (Figure S 12).

(a)

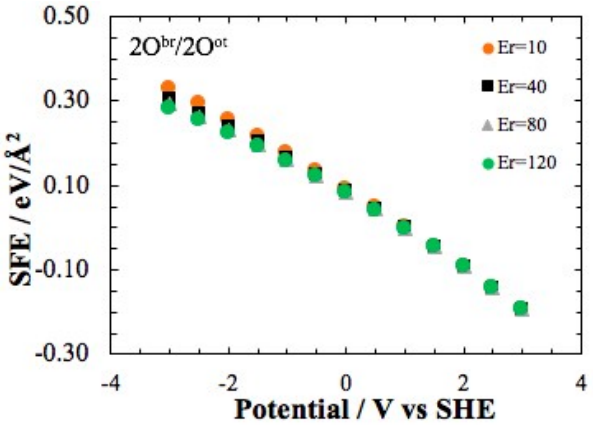

Figure S 12 (Continued next page)

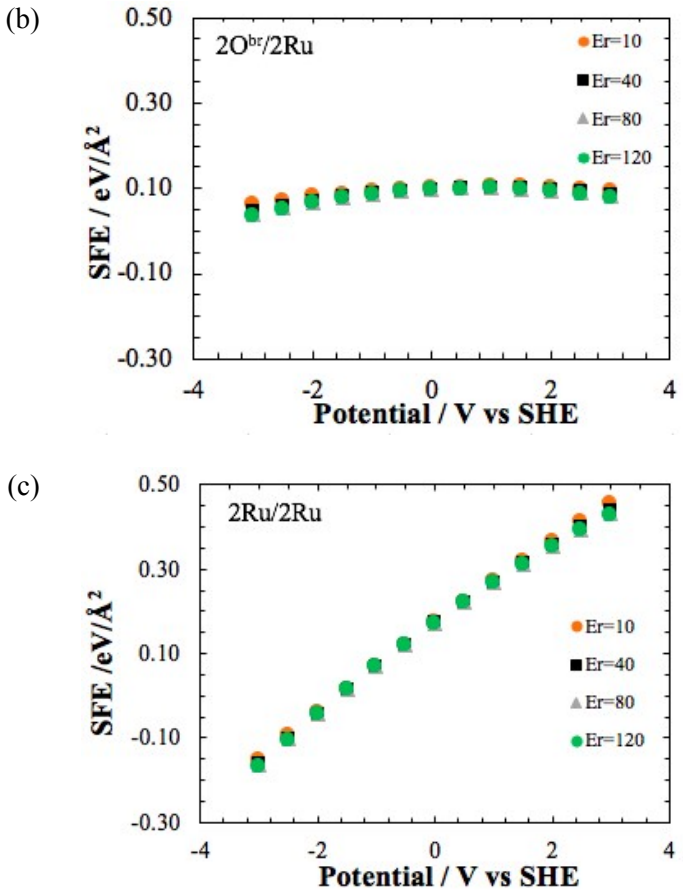

Figure S 12: Relative permittivity effect on surface free energy (SFE) of a) $2O^{br}/2O^{ot}$, b) $2O^{br}/2Ru$ and c) 2Ru/2Ru surface termination of the RuO_2 (110) surface.

5.7 Cavity size test

Similarly, the cavity size test was performed on $2O^{br}/2O^{ot}$, $2O^{br}/2Ru$ and 2Ru/2Ru surface termination of RuO_2 (110) surface and is depicted in Figure S 13. The default value for cavity size is 0.0025 and it can be seen that a minimal variation in SFE value was detected, making the NC_K value used in our DFT calculation reliable.

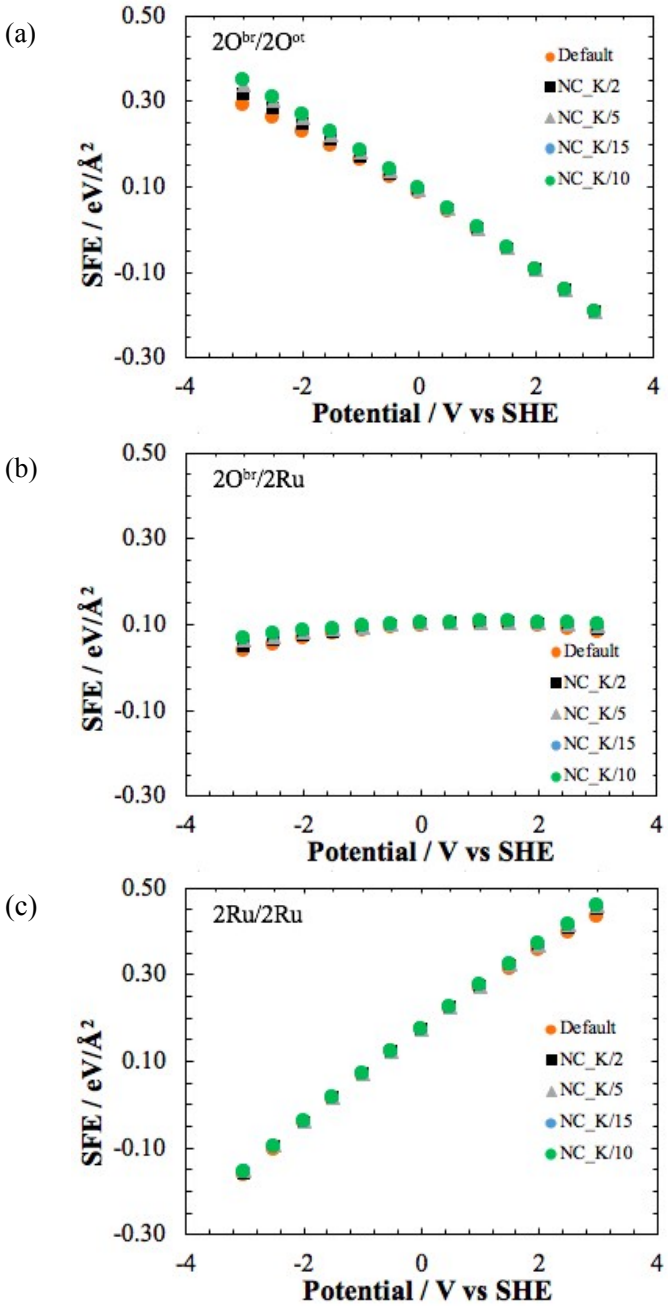

Figure S 13: Cavity size effect on surface free energy (SFE) of $2O^{br}/2O^{ot}$, $2O^{br}/2Ru$ and 2Ru/2Ru surface termination of the RuO_2 (110) surface.

5.8 Potential effect on atoms charge

The charge of bulk and surface Ru and O atoms was calculated and plotted as a function of potential applied. It can be seen that the Ru and O atoms in the bulk do not vary in charge as a function of potential applied. However, on the surface, Ru atoms increase their positive electron charge while O^{ot} and O^{br} 's charge value decrease (in absolute value) as a function of potential applied (Figure S 14).

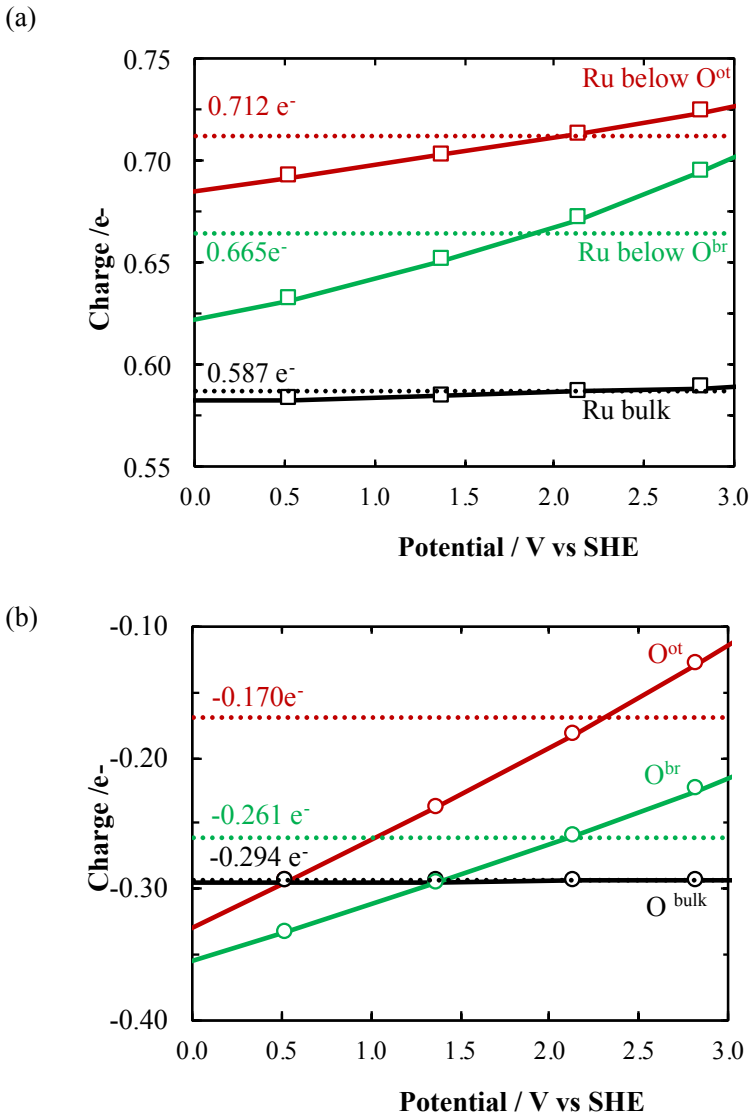

Figure S 14: Charge (e-) variation on Ru and O atoms as a function of potential for RuO_2 (110) surface with $2O^{br}/2O^{ot}$ termination.

5.9 Gibb's energy calculation of the overall slab as a function of potential

In this section, we present the technical background behind the adsorption energy presented as a function of the potential in Eq.6. The relationship between the change in the electronic energy presented as Gibb's energy and the applied electrochemical potential was fitted to parabolas. Then, to find the adsorption energy as a function of potential, we subtracted from the Gibb's energy of the slab containing two ethylene molecules adsorbed symmetrically on the slab, the parabola of the energy of the bare slab and two times the constant ethylene energy that is independent of the potential applied. This value, when divided by two, accounts for the adsorption of one ethylene molecule (Figure S 15).

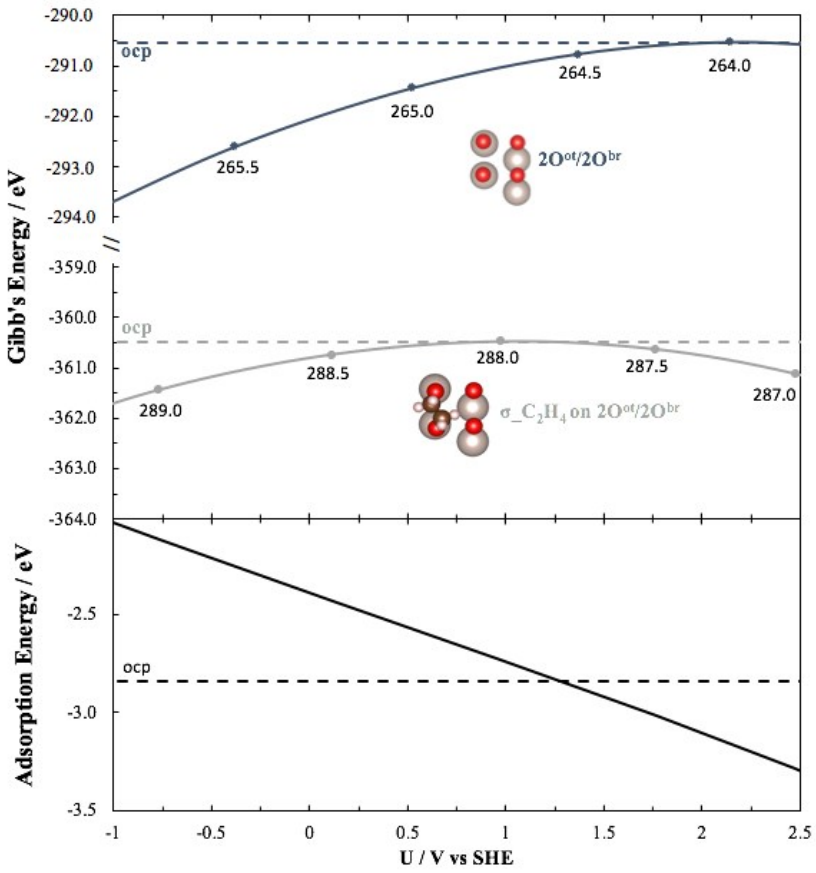

Figure S 15: Effect of potential applied on the Gibb's energy of the pre-adsorption slab and when C_2H_4 is adsorbed in the σ position on the $2O^{ot}$. The subtraction of the two energies is used to find the adsorption energies of the C_2H_4. The labeled points correspond to the computed values at a given surface charge. The half charge interval used for the bare surface is 265.5–264.0 electrons and 289.0–287.0 electrons for the surface with two adsorbed ethylene.

Similarly, the reaction energy is found from subtracting the Gibb's energy parabolas of the initial state from the final state, and the activation energy is found from subtracting that of the initial state from the energy of the transition state (Figure S 16).

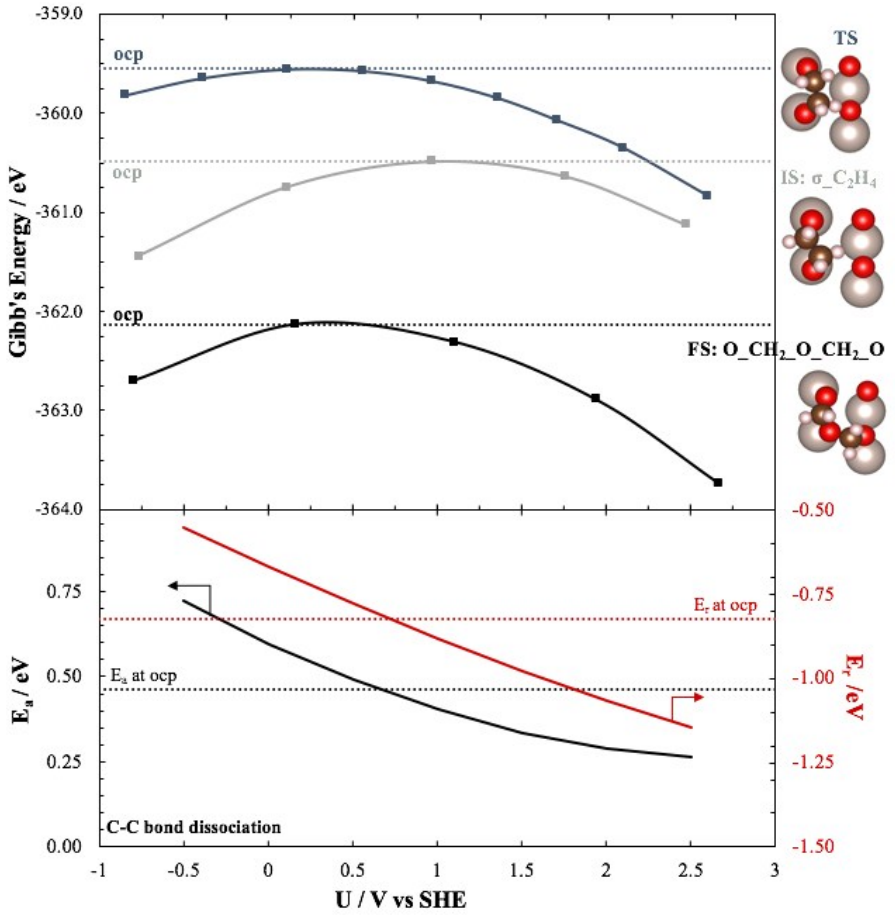

Figure S 16: Effect of potential applied on the Gibb's energy of the initial, transition and final states, used in activation and reaction energies calculations.

5.10 Effect of PBE and HSE functional on the work function of RuO_2(110) surfaces

Additional computations at the HSE level of theory of the work function of the three main surfaces ($2O^{ot}/2O^{br}$, $2Ru/2O^{br}$ and 2Ru/2Ru) show that the PBE work function is in excellent agreement with experimental values (5.8 to 6.6 V) [11], while the HSE results are 0.5 V higher compared to PBE and reach 7.1 V for the $2O^{ot}/2O^{br}$ surface. The 0.5 V difference between HSE and PBE is small enough to ensure that the qualitative mechanistic insight gained in this study does not significantly depend on the theoretical level.

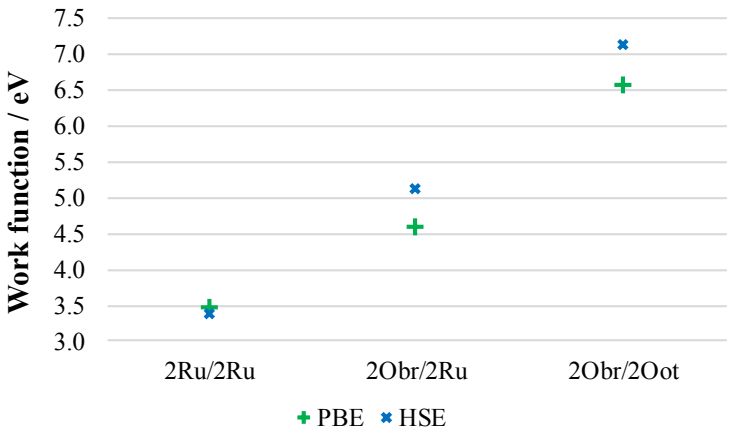

Figure S 17: Work function of the three main surface terminations of RuO_2 as computed with PBE and HSE. The experimental work function for RuO_2 in oxygen is 5.8 to 6.6 V according to [11].

6. Additional Energy Calculations

The potential effect on the adsorption of ethylene in different possible positions is shown in Figure S 18. The C_2H_4 on $2O^{br}/2O^{ot}$ is the most stable at all potential values.

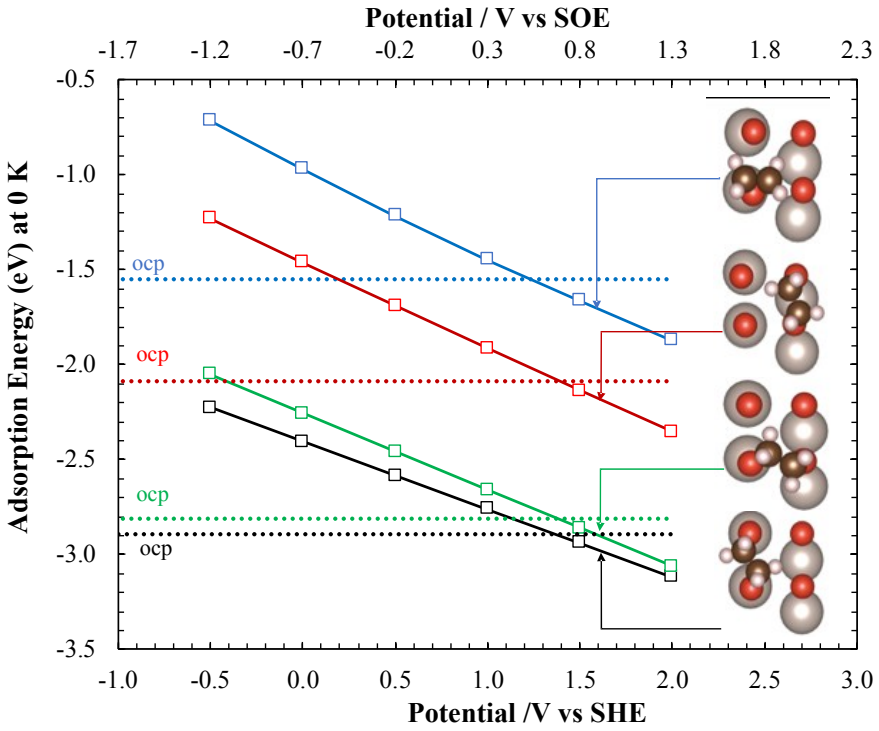

Figure S 18: C_2H_4 adsorption energy at different positions on RuO_2 (110) surface with $2O^{br}/2O^{ot}$ termination. Dotted line corresponds to ocp adsorption value, while the solid line corresponds to adsorption energy variation as a function of potential value.

The C-H dissociation is a possible alternative to C-C bond dissociation; however, its activation energy is slightly higher than that of C-C dissociation. This is shown in Figure S 19.

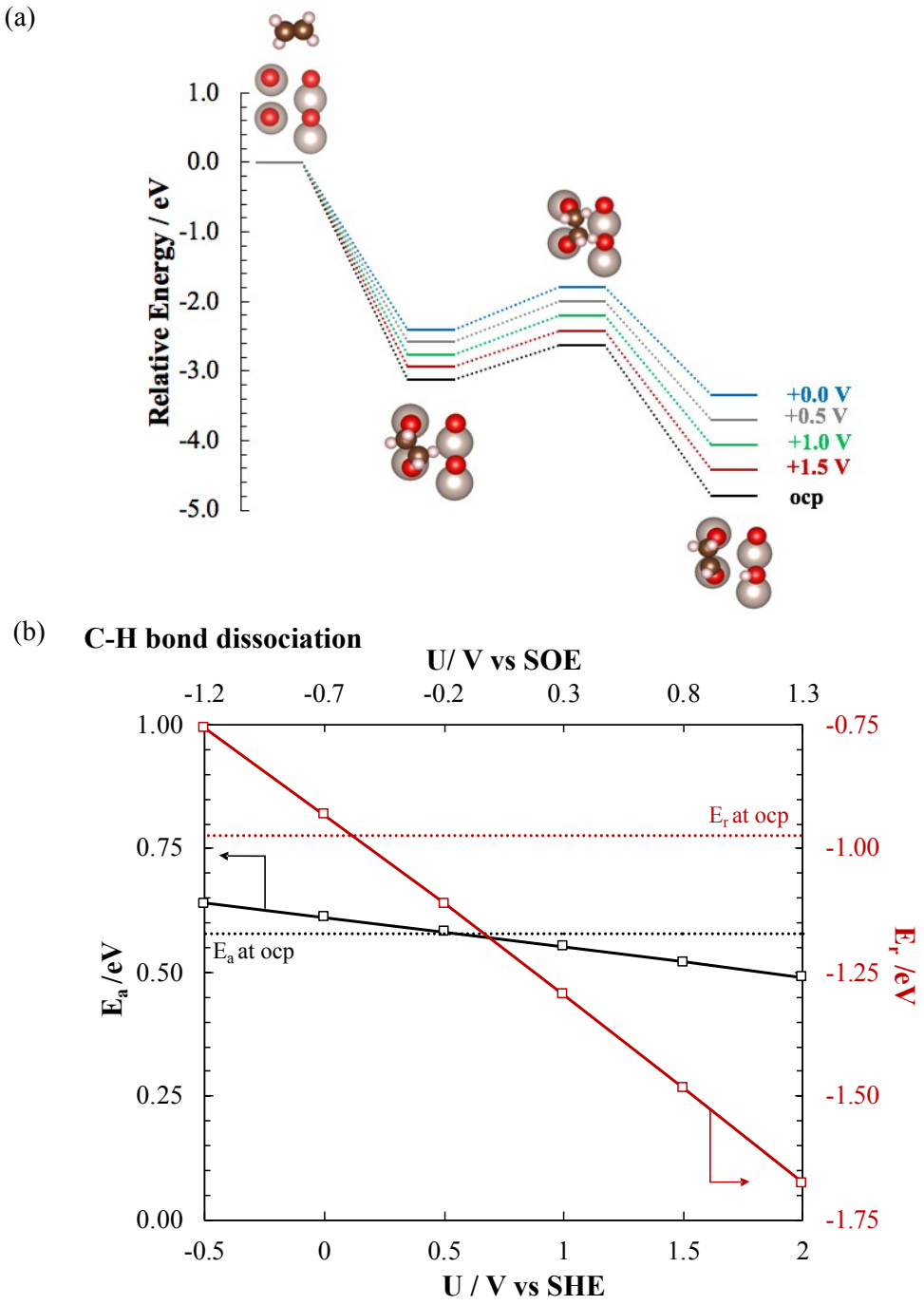

Figure S 19: (a) Energy diagram and (b) corresponding activation and reaction energies as a function of potential for C-H bond dissociation over $2O^{br}/2O^{ot}$ surface termination of RuO_2 (110).

The C-H bond cleavage showed an intermediate C-H bond length of 1.3 Å compared to the initial state of 1.1 Å and the final state of 3.1 Å (Figure S 20).

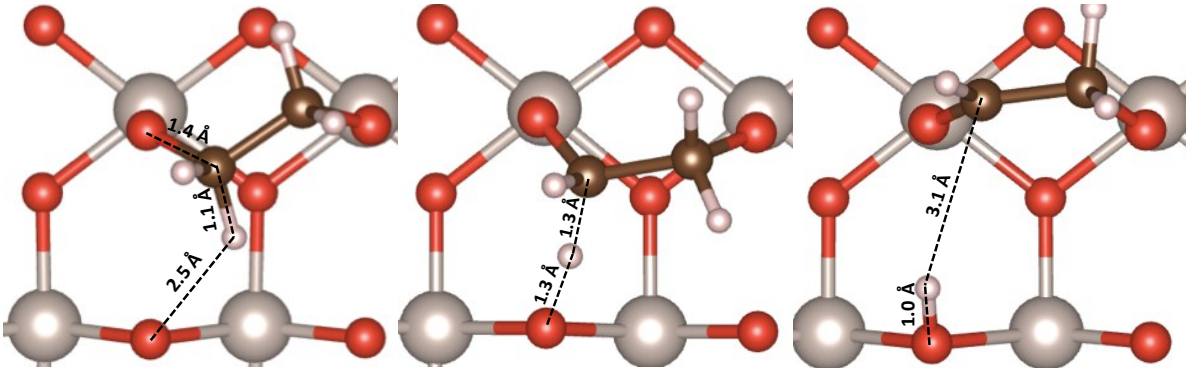

Figure S 20: Structure of the initial, transition and final state of C-H bond rupture on $2O^{br}/2O^{ot}$ RuO_2 (110) surface.

The geometries for oxygen dissociation are given in Figure S 21 where the stretching of the O-O bonds occurs from left to right, with the transition state being in the middle. The distance between the two oxygen stretched from an initial length of 1.4 Å to a final value of 3.1 Å, passing by 1.7 Å at the transition state.

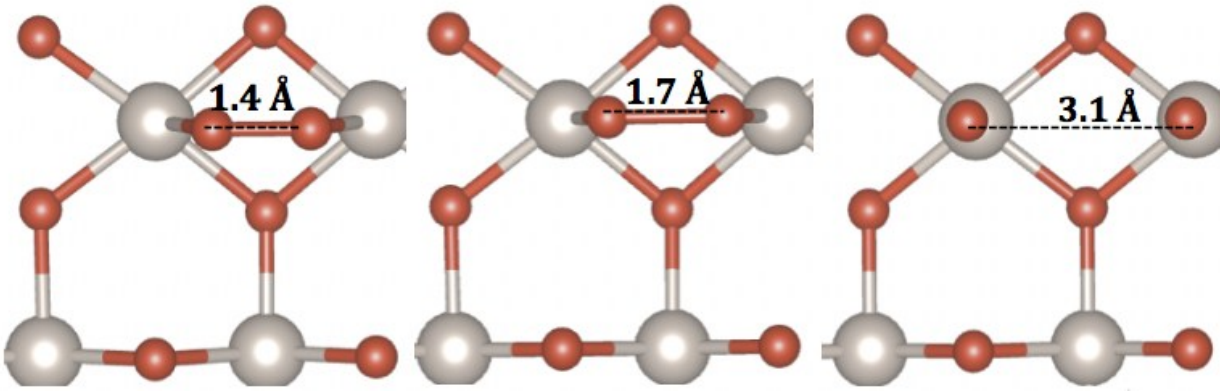

Figure S 21: Structure of the initial, transition and final state of (O-O) bond dissociation on $2O^{br}/2Ru$ RuO_2 (110) surface.

7. References

[1] K. Reuter, M. Scheffler, Phys. Rev. B 65 (2001) 035406.
[2] J. Rossmeisl, A. Logadottir, J.K. Nørskov, Chem. Phys. 319 (2005) 178–184.
[3] C.W. Outhwaite, L.B. Bhuiyan, J. Chem. Soc. Faraday Trans. 2 Mol. Chem. Phys. 79 (1983) 707–718.
[4] L.B. Bhuiyan, C.W. Outhwaite, D. Henderson, J. Chem. Phys. 123 (2005) 034704.
[5] (n.d.).
[6] S.N. Steinmann, P. Sautet, J. Phys. Chem. C 120 (2016) 5619–5623.
[7] K. Mathew, R. Sundararaman, K. Letchworth-Weaver, T.A. Arias, R.G. Hennig, J. Chem. Phys. 140 (2015) 084106.
[8] K. Mathew, R.G. Hennig, ArXiv (2016) 1–6.
[9] D. Tsiplakides, C.G. Vayenas, J. Electrochem. Soc. 148 (2001) E189–E202.
[10] S. Trasatti, Pure Appl. Chem. 58 (1986) 955–966.
[11] A. Böttcher, H. Niehus, Phys. Rev. B - Condens. Matter Mater. Phys. 60 (1999) 14396–14404.